PERGAMON

Acta mater. (2000) 659-674

Acta MATERIALIA

www.elsevier.com/locate/actamat

# HIGH-TEMPERATURE CYCLIC FATIGUE-CRACK GROWTH BEHAVIOR IN AN *IN SITU* TOUGHENED SILICON CARBIDE

**D. CHEN, C. J. GILBERT, X. F. ZHANG and R. O. RITCHIE †**

Materials Sciences Division, Lawrence Berkeley National Laboratory and Department of Materials Science and Mineral Engineering, University of California, Berkeley, CA 94720, USA

*(Received 30 August 1999; accepted 25 October 1999)*

**Abstract** — The growth of fatigue cracks at elevated temperatures (25–1300°C) is examined under cyclic loading in an *in situ* toughened, monolithic silicon carbide with Al-B-C additions (termed ABC–SiC), with specific emphasis on the roles of temperature, load ratio, cyclic frequency, and loading mode (static vs. cyclic). Extensive crack-growth data are presented, based on measurements from an electrical potential-drop crack-monitoring technique, adapted for use on ceramics at high temperatures. It was found that at equivalent stress-intensity levels, crack velocities under cyclic loads were significantly faster than those under static loads. Fatigue thresholds were found to decrease with increasing temperature up to 1200°C; behavior at 1300°C, however, was similar to that at 1200°C. Moreover, no effect of frequency was detected (between 3 and 1000 Hz), nor evidence of creep cavitation or crack bridging by viscous ligaments or grain-boundary glassy phases in the crack wake. Indeed, fractography and crack-path sectioning revealed a fracture mode at 1200–1300°C that was essentially identical to that at room temperature, i.e. predominantly intergranular cracking with evidence of grain bridging in the crack wake. Such excellent crack-growth resistance is attributed to a process of grain-boundary microstructural evolution at elevated temperatures, specifically involving crystallization of the amorphous grain-boundary films/phases. © *2000 Acta Metallurgica Inc. Published by Elsevier Ltd. All rights reserved.*

***Keywords:*** Ceramics; Structural SiC; Mechanical properties (fatigue), High temperature; Grain bridging

## 1. INTRODUCTION

Advanced ceramics offer great potential for a wide range of high-temperature engineering applications where chemical stability at temperatures above 1000°C is required; indeed, this demand for structural materials that can operate at temperatures well above the currently used Ni-base superalloys has precipitated extensive research in ceramics over the past decade [1–7]. In this regard, silicon carbide (SiC) represents one of the attractive candidates because of its combination of high specific strength, and creep and oxidation resistance at elevated temperatures. A serious disadvantage with this ceramic, however, has been its extremely low fracture toughness ($K_c$ ~ 2–3 MPa√m), which severely limits its implementation for most structural applications. Recently though, studies have shown that tougher, more flaw-tolerant, SiC can be processed [8–11] via the formation of heterogeneous microstructures with highly elongated plate-like grains. Indeed, room-temperature toughnesses higher than 9 MPa√m have been reported [8].

Although such advances in the toughening of SiC, and indeed of other ceramics, are impressive, it is the maintenance of such toughness in combination with good elevated-temperature creep and oxidation properties that remains a critical challenge. Moreover, there is still a great deal to be learned about the subcritical crack-growth properties, i.e. by creep and cyclic fatigue, of toughened ceramics, especially at such elevated temperatures. The latter topic is of particular importance as many proposed applications will inevitably involve cyclic loading for prolonged periods of time at high temperatures. Furthermore, since the crack-growth rates, and hence predicted lifetimes, in ceramics are a very strong function of the applied stresses (and stress intensities) [2], design will almost certainly be based on the concept of a threshold stress or stress intensity for no crack growth.

Due primarily to difficulties in experimentation, the vast majority of previous studies on cyclic crack growth in monolithic ceramics has focused on room temperature behavior, primarily in zirconia [12, 13],

---

† To whom all correspondence should be addressed.

1359-6454/00/$20.00
PII: S1359-6454(99)00406-1

alumina ($Al_2O_3$) [14–19], silicon nitride ($Si_3N_4$) [20–24] and SiC [8, 25, 26]. The process of fatigue generally involves the cyclic-loading induced degradation of the extrinsic toughening mechanisms behind the crack tip; in most non-transforming ceramics, the latter derives from crack bridging, by uncracked ligaments or interlocking grains in monolithic systems [25, 27, 28] and by intact whisker, fibers or particles in composite materials [29]. Frictional-wear models [14, 30] have been proposed to account for such behavior. Specifically, repetitive sliding wear along the boundaries of active bridging sites results in premature debonding of grains under cyclic loading which reduces the frictional pullout stresses; this in turn lowers the toughening capacity of grain-bridging zones and enhances the *local* crack-tip driving forces, thereby promoting accelerated crack-growth rates [14, 16, 20, 26, 31, 32]. Since the crack-advance mechanism is unchanged from that under static loading, ambient-temperature fatigue-crack growth rates generally exceed those under static loads at equivalent applied stress intensities [2, 15, 17, 18, 21, 23, 25], and display a marked dependency on the maximum stress intensity, $K_{max}$; moreover, growth rates are likely to be insensitive to the cyclic frequency.

In comparison, far less is understood about cyclic fatigue mechanisms at elevated temperatures; moreover, much of the published data, on nitride- and oxide-based monolithic and composite ceramics [33–43], appears to be contradictory. Most studies report lower crack-growth rates and hence longer lifetimes under cyclic, compared to sustained, loading [33–36], i.e. the opposite of behavior observed at ambient temperature. However, three separate studies on hot-pressed or HIPed $Si_3N_4$ conclude that cyclic crack-growth rates between 1370 and 1450°C are faster [37], slower [34], or the same [38] as corresponding growth rates under static loads at equivalent stress-intensity levels. Several studies have reported slower growth rates, and hence increased lifetimes, at higher loading frequencies [33, 34, 39, 44], yet contrary studies for $Si_3N_4$ at 1400$^o$C claim no discernible effect of frequency and indeed no correlation between growth rates and the stress-intensity factor [39]. Moreover, results for monolithic and reinforced $Si_3N_4$ suggest that cyclic crack-growth rates are both time- and cycle-dependent [39].

Despite such contradictions, the primary mechanisms of high-temperature crack growth are generally attributed to softening and nonlinear deformation through cavitation along interfaces due to viscous flow of the grain-boundary glassy phase; cavity growth and linkage then creates a microcracked region ahead of the crack tip which acts as the origin of permanent crack-tip damage and provides apparent stability for subcritical crack growth [40, 44]. The presence of glassy phase can produce crack-bridging ligaments, both as individual ligaments [45] or as a viscous grain-boundary film during grain bridging [46]. The force produced across crack faces by such viscous bridging can reduce the local crack-tip stress intensity, leading to slower, yet rate-dependent, growth rates under cyclic loading.

As the viscosity of glass phase depends strongly on its composition, thermal stability, oxidation and degree of crystallization, in addition to the temperature and strain rate (frequency), the balance between intrinsic damage, in the form of softening and creep cavitation within the glassy phase, and extrinsic crack-tip shielding from viscous bridging will be extremely sensitive to the precise conditions involved. It is believed that the marked differences in the experimental results reported to date are a manifestation of this sensitivity, specifically in the varying size and chemistry of the grain-boundary phase in differing ceramic systems, temperature and frequency regimes.

Since no work to date has examined this question of elevated-temperature cyclic crack growth in SiC ceramics, the principal goal of the present study is to elucidate the microstructural damage and corresponding shielding mechanisms in an *in situ* toughened silicon carbide with known high strength and toughness properties at ambient temperatures [8, 25]. Specifically, the role of critical variables such as temperature (25–1300°C), frequency (3–1000 Hz), and load ratio (ratio of minimum to maximum loads, $R = 0.1–0.5$) are examined with the objective of discerning the salient micro-mechanisms and microstructural factors controlling high-temperature cyclic fatigue in SiC ceramics.

## 2. EXPERIMENTAL PROCEDURES

### 2.1. *Material processing and microstructure*

The monolithic silicon carbide under study was processed with Al–B–C additions, and is termed ABC–SiC. The material was prepared using submicrometer β-SiC, which was mixed with 3 wt% of Al, 0.6 wt% of B, and 2 wt% of C. After cold die-compression at 35 MPa, the green compact was hot pressed to a relative density of ~ 99 % in a graphite furnace at 1900$^o$C for 1 h at a pressure of 50 MPa under flowing argon.

The resulting microstructure consisted of 5 vol.% β-SiC (cubic polytype 3C) and 95 vol.% α-SiC (49 vol.% 4H and 46 vol.% 6H hexagonal polytype). The morphology of the microstructure shows a three-dimensional interlocking network of elongated plate-like grains with aspect ratio of ~3.5 (Fig. 1). Additionally, an Al- and O-containing amorphous film, ~1 nm thick, was observed along grain boundaries; strips of crystalline triple-junction phase, identified by electron diffraction as $Al_8B_4C_7$, $Al_4O_4C$ and $Al_2O_3$, were also noticed on fracture surfaces in the as-hot-pressed state. More details on the processing and microstructural characterizations of this class of SiC materials have been reported elsewhere [8, 25]. Ambient temperature mechanical-property evaluation for this microstructure gave a four-point bend strength of 620 (±15) MPa and a fracture toughness $K_c$ of 6.2 MPa√m, the latter being measured using a fatigue pre-cracked compact-tension DC(T) specimen.

High-resolution transmission electron microscopy (TEM) was performed to examine the nature of the grain boundaries. Moreover, by taking specimens in the vicinity of the crack tip, an attempt was made to discern the salient microstructural damage mechanisms responsible for crack advance for both slow crack growth under both static and cyclic loading. Specifically, 3-mm diameter TEM foils were taken from the crack-tip region of fracture and fatigue test specimens such that the crack line was parallel to the axis of the foil with the crack tip located ~500 μm away from the foil center. The foils, which were ground down to 20 μm using a precision dimpling machine and further thinned by argon ion milling, were examined on a Philips CM200 microscope, operating at 200 kV.

### *2.2. Cyclic fatigue-crack growth rate measurements*

Cyclic fatigue-crack growth testing was performed using disk-shaped DC(T) specimens, containing "large" (> 3 mm) through-thickness cracks; the test pieces conformed to an ASTM E-647 standard geometry, with a width of ~28 mm and thickness of ~3 mm. Samples were cycled at 850, 1200 and 1300°C, and behavior compared to that at room temperature (RT=25°C). Tests were conducted at load ratios of $R = 0.1$ and 0.5 at frequencies, ν, between 25 and 1000 Hz at room temperature and between 3 and 25 Hz at elevated temperatures (sinusoidal waveform). For comparison, testing under sustained loading (static fatigue/creep) was carried out at room temperature and at 1300°C, with the stress intensity held at the same $K_{max}$ level used in the cyclic tests.

All experiments were conducted on MTS computer-controlled servo-hydraulic mechanical testing machines. Elevated temperature tests were performed in an environmental chamber/furnace with graphite elements that maintain temperature to within ±1°C. Heating and cooling rates were kept at 10°C/min to minimize any thermal shock effects. After reaching the desired temperature, the furnace temperature was kept constant for 1–3 h before starting the test to allow the thermal equilibrium of the system. The test environment at elevated temperatures was flowing gaseous argon at atmospheric pressure; (except where specified) corresponding room temperature tests were conducted in air. Testing at 1000 Hz was performed on a MTS servo-hydraulic test frame using a voice-coil serovalve [47].

Cyclic tests were performed in general accordance with ASTM standard E-647. Specifically, samples were cycled under automated stress-intensity $K$ control while maintaining constant load ratio. To approach the fatigue threshold stress-intensity values, $\Delta K_{th}$ and $\Delta K_{max,th}$, growth rates were monitored under decreasing $\Delta K$ conditions, with a normalized $K$-gradient set to –0.08 mm $^{-1}$; the value of $\Delta K_{th}$, below which large cracks are presumed to be dormant, was operationally defined at a maximum growth rate of $10^{-10}$ m/cycle. The use of the stress intensity $K$ at elevated temperatures was justified through considerations of the relative dominance of

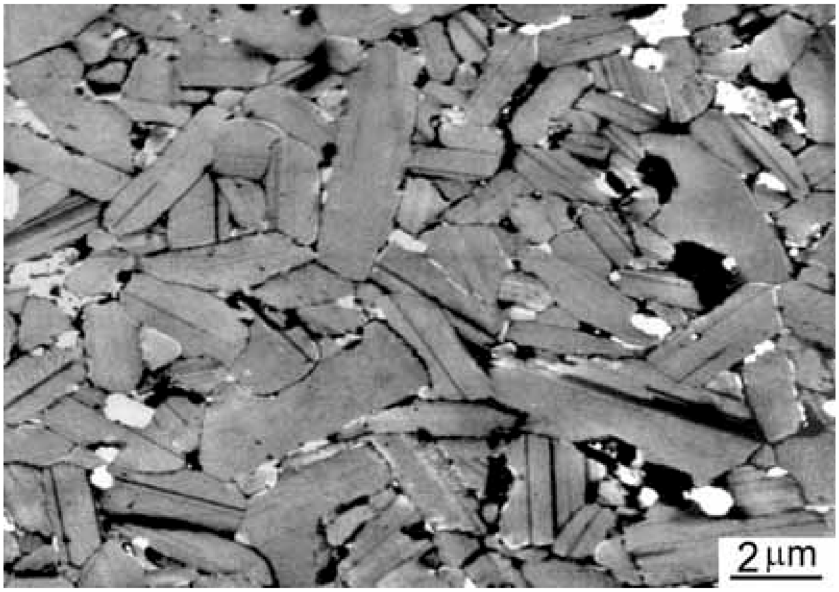

Fig. 1. Representative microstructure of the ABC–SiC, treated by thermal etching at 1800°C for 1h, illustrating elongated, plate-shaped interlocking grains with mean size of 5.2 (± 2.1) μm long and 1.5 (± 0.5) μm wide.

small-scale creep conditions, as described in Appendix A.

At ambient temperature, crack lengths were continuously monitored using unloading elastic-compliance measurements with a 350 Ω strain gauge attached to the back-face of the specimen. However, a key component of this work was the use of an electrical potential-drop technique to continuously monitor crack lengths *in situ* at elevated temperatures. To our knowledge, this is the first time such a technique has been used for high-temperature measurements in ceramics, and is made possible in the present case by the electrical conductivity of ABC-SiC at these temperatures (the resistivity above 600°C is ~10 Ω cm). This method presents several significant advantages over the techniques used to date, which have involved periodic interruptions of the test to cool the sample to make optical or compliance measurements, both in avoiding artificial effects due to thermal fatigue and oxidation from repeated exposure to air and in efficiency of measurement. In the present tests, a constant direct current of ~400–800 mA was introduced into the sample, such that an initial output potential of between ~0.4 and 1.0 V was developed across the notch mouth. Subsequent changes in this potential were then continuously measured to permit *in situ* monitoring of crack length. Using this approach, it is possible in principle to monitor changes in crack length to a resolution of 20–40 μm. Further details on this method as applied to SiC are given in the Appendix B. Both elastic back-face strain compliance and electrical-potential calibrations for this specimen geometry are given in Ref. [48].

## 3. EXPERIMENTAL RESULTS

### *3.1. Fatigue-crack growth behavior*

*3.1.1 Ambient-temperature behavior.* The variation in fatigue-crack growth rates, d*a*/d*N*, with applied stress-intensity range, $\Delta K$, for ABC-SiC at 25°C is shown in Fig. 2 for environments of room air and flowing argon gas (at $R = 0.1$, $\nu = 25$ Hz). It is apparent that there is a negligible difference between behavior in air and an inert gas atmosphere at ambient temperatures; both environments show a relatively high fatigue threshold of $\Delta K_{th}$ ~ 5.1 MPa$\sqrt{m}$, which is approximately 80% of $K_c$.

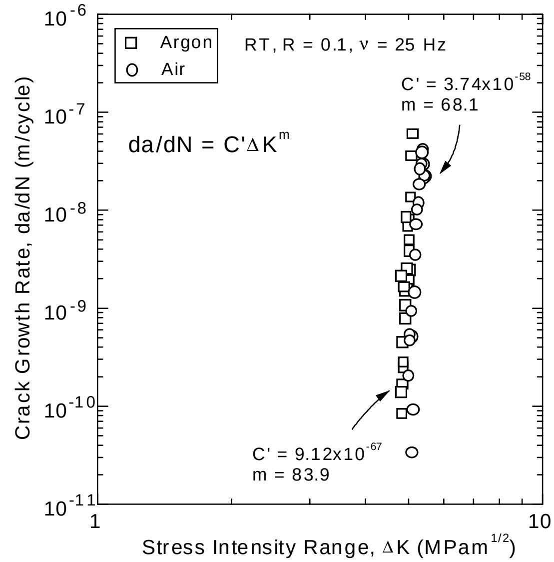

Fig. 2. Room-temperature cyclic fatigue-crack growth rates, d*a*/d*N*, in ABC–SiC, as a function of the applied stress-intensity range $\Delta K$, showing a negligible difference in behavior in room air and gaseous argon environments.

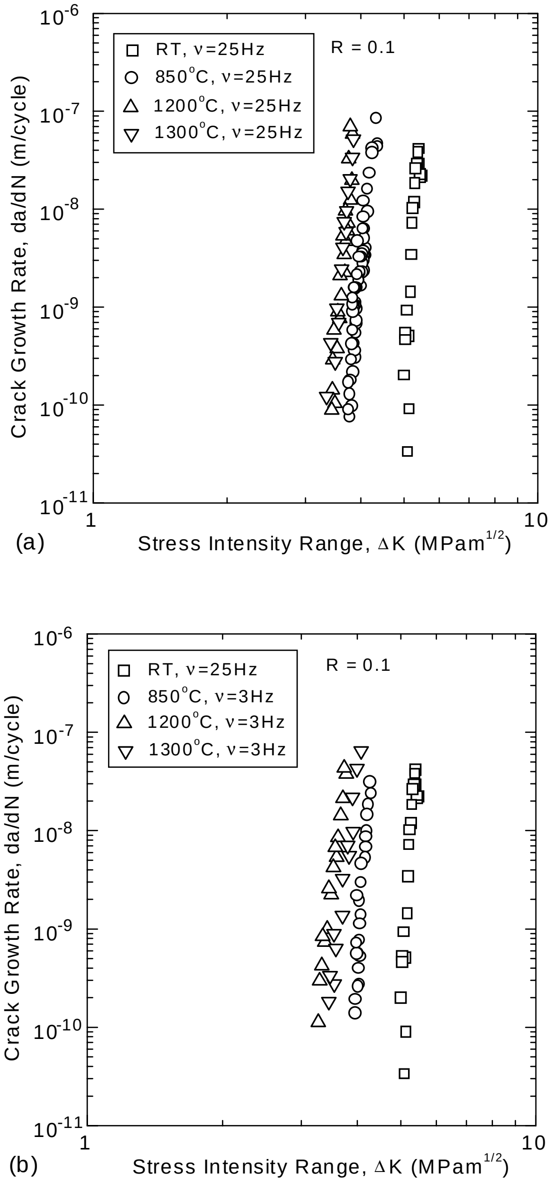

Fig. 3. Cyclic fatigue-crack growth rates, d*a*/d*N*, at $R = 0.1$ in ABC–SiC, as a function of the applied stress-intensity range $\Delta K$ at temperatures between 25 and 1300°C at frequencies of (a) 25 Hz and (b) 3 Hz.

Table 1. Cyclic fatigue-crack growth properties for ABC–SiC

| Load ratio and frequency | Testing temperature (°C) | Fatigue thresholds | | Paris-law fit parameters, $da/dN = C'\Delta K^m$ | |
|---|---|---|---|---|---|
| | | $\Delta K_{th}$ (MPa$\sqrt{m}$) | $K_{max,th}$ (MPa$\sqrt{m}$) | $m$ | $C'$ (m/cycle) (MPa$\sqrt{m}$)$^{-m}$ |
| $R = 0.1$ | 25 | 5.14 | 5.71 | 68.1 | $3.74 \times 10^{-58}$ |
| $\nu = 25$ Hz | 850 | 3.71 | 4.12 | 39.0 | $6.19 \times 10^{-32}$ |
| | 1200 | 3.32 | 3.69 | 52.3 | $5.66 \times 10^{-37}$ |
| | 1300 | 3.54 | 3.93 | 44.4 | $4.25 \times 10^{-34}$ |
| $R = 0.1$ | 850 | 3.85 | 4.28 | 59.1 | $2.46 \times 10^{-44}$ |
| $\nu = 3$ Hz | 1200 | 3.43 | 3.81 | 37.4 | $0.94 \times 10^{-29}$ |
| | 1300 | 3.66 | 4.07 | 35.2 | $1.42 \times 10^{-29}$ |
| $R = 0.5$ | 25 | 2.98 | 5.96 | 92.5 | $1.29 \times 10^{-54}$ |
| $\nu = 25$ Hz | 1300 | 2.12 | 4.24 | 82.8 | $1.14 \times 10^{-37}$ |

Characteristic of ceramic materials at low temperatures [2], growth rates display a marked sensitivity to the stress intensity. In terms of a simple Paris power-law formulation:

$$da/dN = C'\Delta K^{m}, \qquad (1)$$

where $C'$ and $m$ are scaling constants, these data show a Paris exponent $m$ between 68 and 84.

*3.1.2. Effect of temperature.* The variation in fatigue-crack growth rates at temperatures of 850, 1200 and 1300°C at $R = 0.1$ is shown in Fig. 3 for two loading frequencies of $\nu$=25 and 3 Hz. The $da/dN$ vs $\Delta K$ data were fitted to a simple Paris formulation [equation (1)]; values of the exponents $m$ and prefactor $C'$, together with the respective $\Delta K_{th}$ and $\Delta K_{max,th}$ threshold stress intensities, are listed in Table 1.

It can be seen that at both frequencies, growth rates are increased and the $\Delta K_{th}$ thresholds decreased with increasing temperature up to 1200°C, although the slope of the growth-rate curves remains roughly similar. The decrement in $\Delta K_{th}$ with increasing temperature is more pronounced from 25 to 850°C (~28%) than that from 850 to 1200°C (~11%); moreover, no further decline in crack-growth resistance is apparent at 1300°C.

*3.1.3. Effect of loading frequency.* The effect of loading frequency is examined in Fig. 4 at $R = 0.1$. No effect is seen between 25 and 1000 Hz at room temperature; this is to be expected as both the predominant damage (intergranular cracking) and shielding (grain bridging) mechanisms at low temperatures are both essentially rate-insensitive. However, in contrast to silicon nitride ceramics [35], no effect of loading frequency, between 3 and 25 Hz, is apparent at elevated temperatures either. This implies that cracking is still cycle-dependent, and not time-dependent, as might be expected at these temperatures if creep damage or viscous shielding mechanisms were active.

*3.1.4. Effect of load ratio.* Cyclic fatigue-crack growth rates in ABC–SiC at 25 and 1300°C are plotted in Fig. 5 as a function of the stress-intensity range $\Delta K$ and maximum stress intensity $K_{max}$ for load ratios of 0.1 and 0.5. It is apparent that behavior is similar at both low and high temperatures: $\Delta K_{th}$ thresholds are reduced by ~40%, and growth rates *at fixed ΔK* are increased with increasing load ratio (Fig. 5(a)), whereas $K_{max,th}$ thresholds and subsequent growth rates are almost identical at $R$ = 0.1 and 0.5 when compared as a function of $K_{max}$.

Such behavior is typical of many ceramics at lower temperatures and indicates that fatigue-crack growth rates are a much stronger function of $K_{max}$ than $\Delta K$ (e.g. Refs[19, 20, 23, 25, 32, 49]). This can be seen by expressing the growth-rate data in Fig. 5 in terms of a modified Paris power-law relationship, which includes the effect of both $\Delta K$ and $K_{max}$ [49], viz.

$$da/dN = C\,(K_{max})^{n}\,(\Delta K)^{p}, \qquad (2)$$

where, compared to equation (1), $C = C'(1-R)^{n}$ and $n$ and $p$ are experimentally determined crack-growth exponents such that nominally $(n + p) = m$. A regression fit to the data in Fig. 5, in units of m/cycle and MPa√m, yields:

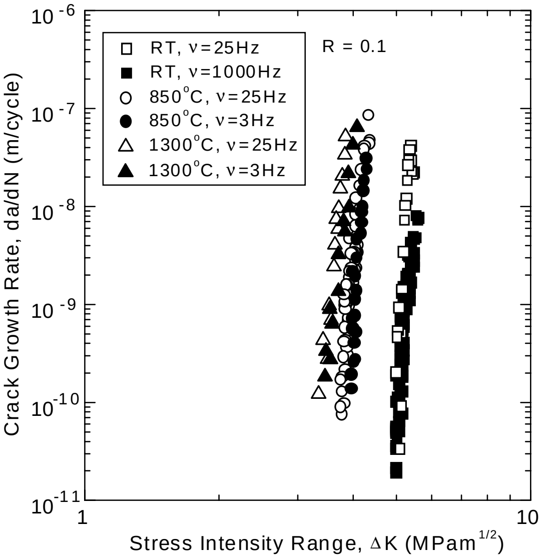

Fig. 4. Influence of loading frequency (3–1000 Hz) on cyclic fatigue-crack growth rates, $da/dN$, in ABC–SiC as a function of the applied stress-intensity range, $\Delta K$, for the tests conducted at $R = 0.1$ at temperatures between 25 and 1300°C.

$$\mathrm{d}a/\mathrm{d}N = 5.9\times10^{-73}\,(K_{\max})^{75.3}(\Delta K)^{8.6} \text{ at } 25°\mathrm{C}\,, \tag{3a}$$

$$\mathrm{d}a/\mathrm{d}N = 3.3\times10^{-61}\,(K_{\max})^{73.7}(\Delta K)^{13.2} \text{ at } 1300°\mathrm{C}\,. \tag{3b}$$

The large $K_{\max}$ dependence is also reflected in the increase in slope at higher load ratios when the data are characterized in terms of $\Delta K$. Specifically, with increasing $R$ from 0.1 to 0.5, values of the exponent $m$ in equation 1 are increased from ~68 to 93 at 25°C, and from 44 to 83 at 1300°C (Table 1).

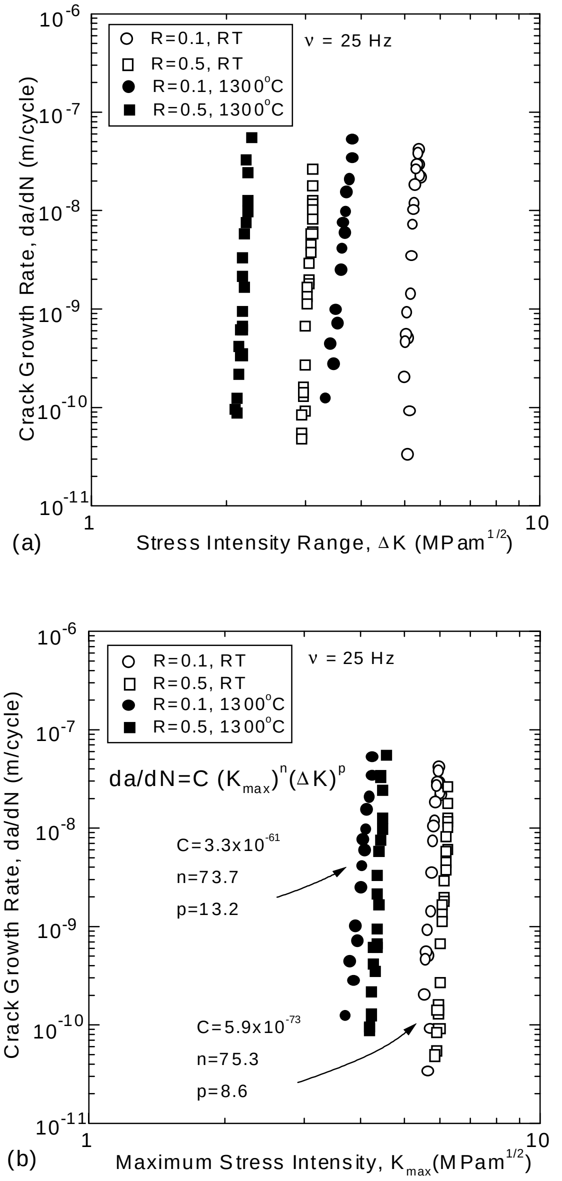

Fig. 5. Variation of cyclic fatigue-crack growth rates, d$a$/d$N$, at $R$ = 0.1 and 0.5 with (a) $\Delta K$ and (b) $K_{\max}$, in ABC–SiC at 25 and 1300°C, showing a large growth-rate dependence on $K_{\max}$ relative to $\Delta K$.

*3.1.5. Effect of static vs cyclic loading.* Similar to zirconia [12, 13], alumina [19] and silicon nitride [20], cyclic fatigue crack-growth rates in the ABC–SiC at ambient temperature were significantly faster than corresponding (static fatigue) crack-growth rates under sustained loading at equivalent stress-intensity levels, i.e. compared at a $K_{\mathrm{I}}$ in static fatigue identical to $K_{\max}$ in cyclic fatigue (Fig. 6) for an applied constant $K_{\max}$ of 5.9 MPa√m at 25°C. This is consistent with the fact that at low temperatures, the crack-advance (damage) mechanisms are identical under cyclic and static loading; it is the cyclic-loading induced degradation in wake shielding that accelerates the growth rates under cyclic loads. In contrast, behavior at elevated temperatures is generally the opposite as the sustained-load mechanism, i.e. creep, involving softening and cavitation in the grain-boundary films, is generally far more damaging [40]. However, for the present ABC–SiC, this is clearly not the case. A similar comparison at 1300°C of growth rates under static and cyclic loads, at an applied constant $K_{\max}$, reveals behavior similar to that at 25°C, i.e. significantly faster crack-growth rates under cyclic loads.

## *3.2. Microstructural characterizations*

*3.2.1. Fracture surface.* Scanning electron microscopy of room-temperature overload fracture surfaces in ABC–SiC (Fig. 7) revealed a predominantly intergranular fracture characteristic of many grain-bridging ceramics. Corresponding fatigue frac-

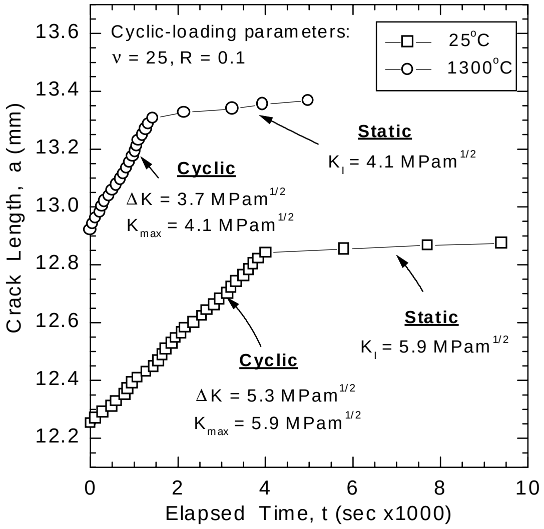

Fig. 6. Crack length, $a$, plotted as function of time, $t$, demonstrating the effect of sustained loading conditions vs cyclic loading conditions, at a fixed maximum stress intensity $K_{\mathrm{I}} = K_{\max}$. Plotted are behavior at 25°C, where $K_{\mathrm{I}} = K_{\max}$ = 5.9 MPa√m, and at 1300°C, where $K_{\mathrm{I}} = K_{\max}$ = 4.1 MPa√m. Note the increase in growth rates under cyclic, compared to static, loading at both low and high temperatures.

ture surfaces at 25°C (Fig. 8) display a similar intergranular morphology with the notable exception of the presence crack-surface damage and extensive debris. As reported previously for ABC–SiC [25, 26], such debris is formed by wear and abrasion of the crack faces during cycling, consistent with the frictional wear degradation of the grain-bridging zone. Fracture surfaces were identical at loading frequencies of 25 and 1000 Hz.

Corresponding fatigue fracture surfaces at 1300°C also show a predominantly intergranular fracture covered with debris, with no apparent change at 3 and 25 Hz (Fig. 9). Indeed, these fracture surfaces are remarkably similar to those at 25°C, and again imply an intergranular crack-advance mechanism coupled with frictional wear degradation of the grain-bridging zone in the crack wake. In stark contrast to the elevated temperature behavior of silicon nitride [37, 39], alumina [33] and silicide-matrix composites [44], no evidence of the grain-boundary glassy phase, viscous bridging or cavitated grain boundaries, indicative of creep damage, is evident on fracture surfaces in this material up to 1300°C.

*3.2.2 Crack paths.* Metallographic sections taken perpendicular to the crack surfaces confirm the intergranular crack paths, the existence of grain bridging, and the presence of debris inside the crack during ambient temperature fatigue-crack growth, as shown in Fig. 10 for frequencies of 25 and 1000 Hz. At 1300°C, crack paths show a similar nature (Fig. 11) with clear evidence of grain bridging and no evidence of microcracking zones, cavitation or viscous-phase bridging, as is often observed in $Al_2O_3$ and $Si_3N_4$ ceramics at these temperatures [33, 37, 39, 44].

Transmission electron microcopy studies on regions in the immediate vicinity of the crack tip provided direct confirmation of these observations. Akin to behavior at room temperature, for both static and cyclic crack growth, crack extension was predominantly along the grain boundaries with no indication of cavitation damage near the crack tip nor viscous-phase bridging in the crack wake (Fig. 12). Similar behavior was seen at 850 and 1200°C.

*3.2.3. Grain-boundary structure.* As noted above, high-resolution transmission electron microscopy clearly shows a small, ~1 nm thick, amorphous film along grain boundaries in the as-processed condition (Fig. 13(a)). However, due to thermal exposure during high-temperature fatigue testing, this glassy film fully crystallizes, as shown in Fig. 13(b) following pre-exposure for 72 h at 1300°C. As the newly formed crystallized phase is < 1 nm thick, it is difficult to discern its identify or crystal structure; however, its chemical composition is unchanged during crystallization.

## 4. DISCUSSION

### 4.1. Crack-growth behavior

The characteristics of cyclic fatigue-crack propagation in ABC–SiC at elevated temperatures (850–1300°C) appear to be unique compared to $Al_2O_3$ and $Si_3N_4$ ceramics. Similar to the latter materials, growth rates are indeed accelerated, and fatigue thresholds are decreased, with increasing temperature. However, in contrast to these materials:

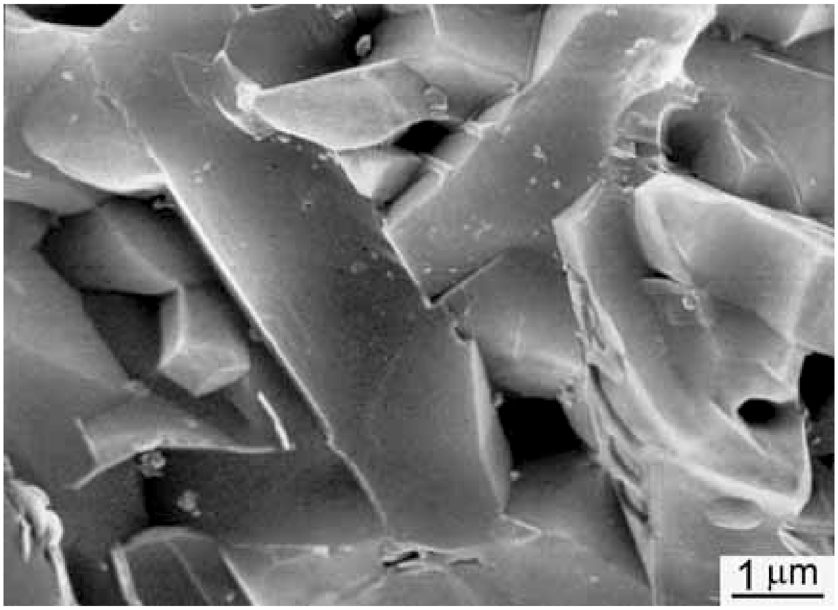

Fig. 7. Scanning electron micrograph of the fracture morphology of overload fracture in ABC–SiC testing at room temperature, showing a primarily intergranular mode of fracture.

- no further acceleration in growth rates, and no further degradation in thresholds, is seen at 1300°C, compared to behavior at 1200°C;
- there is no apparent frequency effect on crack-growth rates, identical to behavior at ambient temperatures;
- there is no evidence of creep damage, i.e., from softening and/or cavitation within the grain-boundary phase, nor crack bridging by viscous films or ligaments;
- fractography, crack-path sectioning and crack-tip TEM imaging are all consistent with a predominantly brittle intergranular crack-advance mechanism and the frictional degradation of grain bridging in the crack wake, similar to behavior at ambient temperatures;
- crack velocities under cyclic loading are faster than those under static loading when loaded at equivalent stress-intensity levels.

Such characteristics strongly imply that the damage and shielding mechanisms associated with fatigue-crack propagation in the ABC–SiC ceramic are

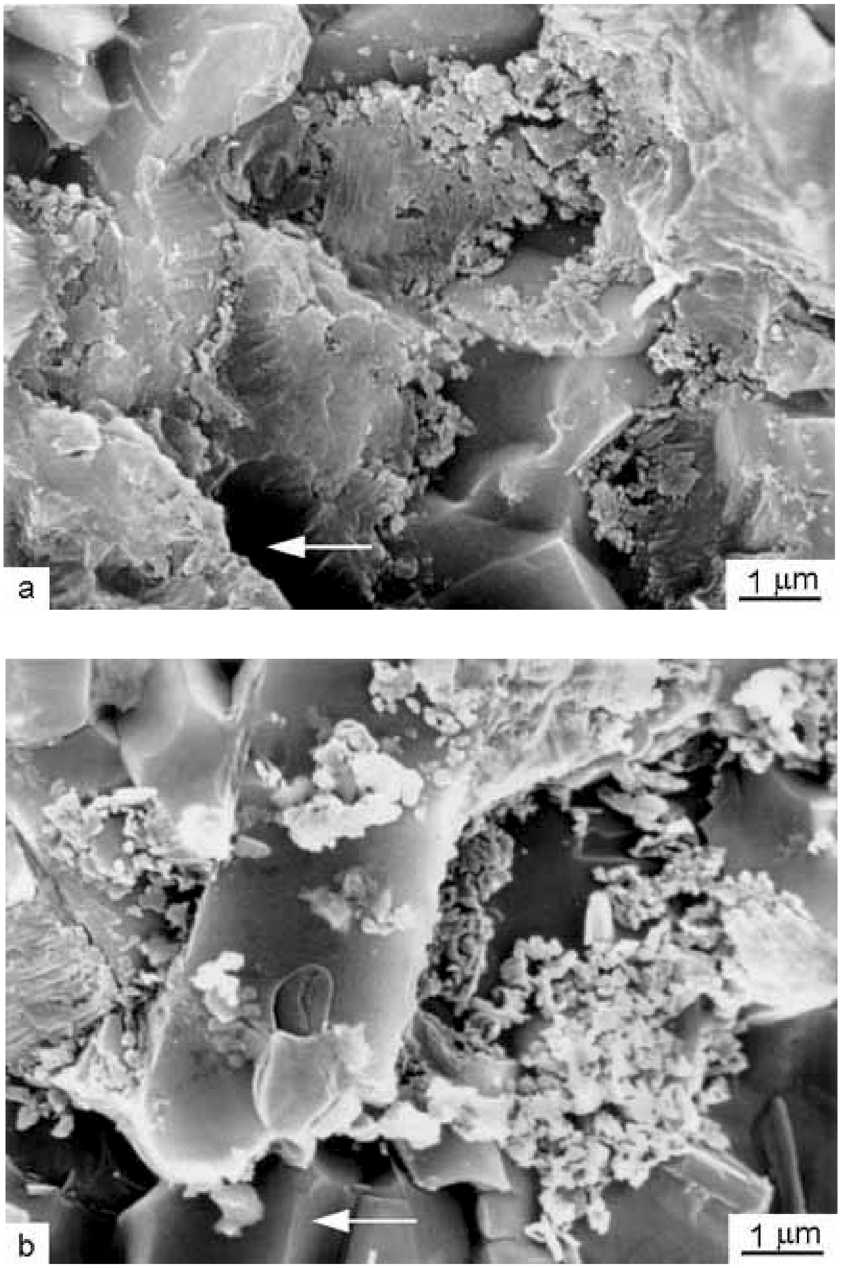

Fig. 8. Scanning electron micrographs of fatigue fracture surfaces in ABC–SiC at room temperature ($R$ = 0.1) for frequencies of (a) 25 Hz and (b) 1000 Hz. Note in comparison to Fig. 7, the extensive crack surface debris, consistent with the frictional wear degradation of the grain-bridging zone under cyclic loading. Arrow indicates direction of crack growth.

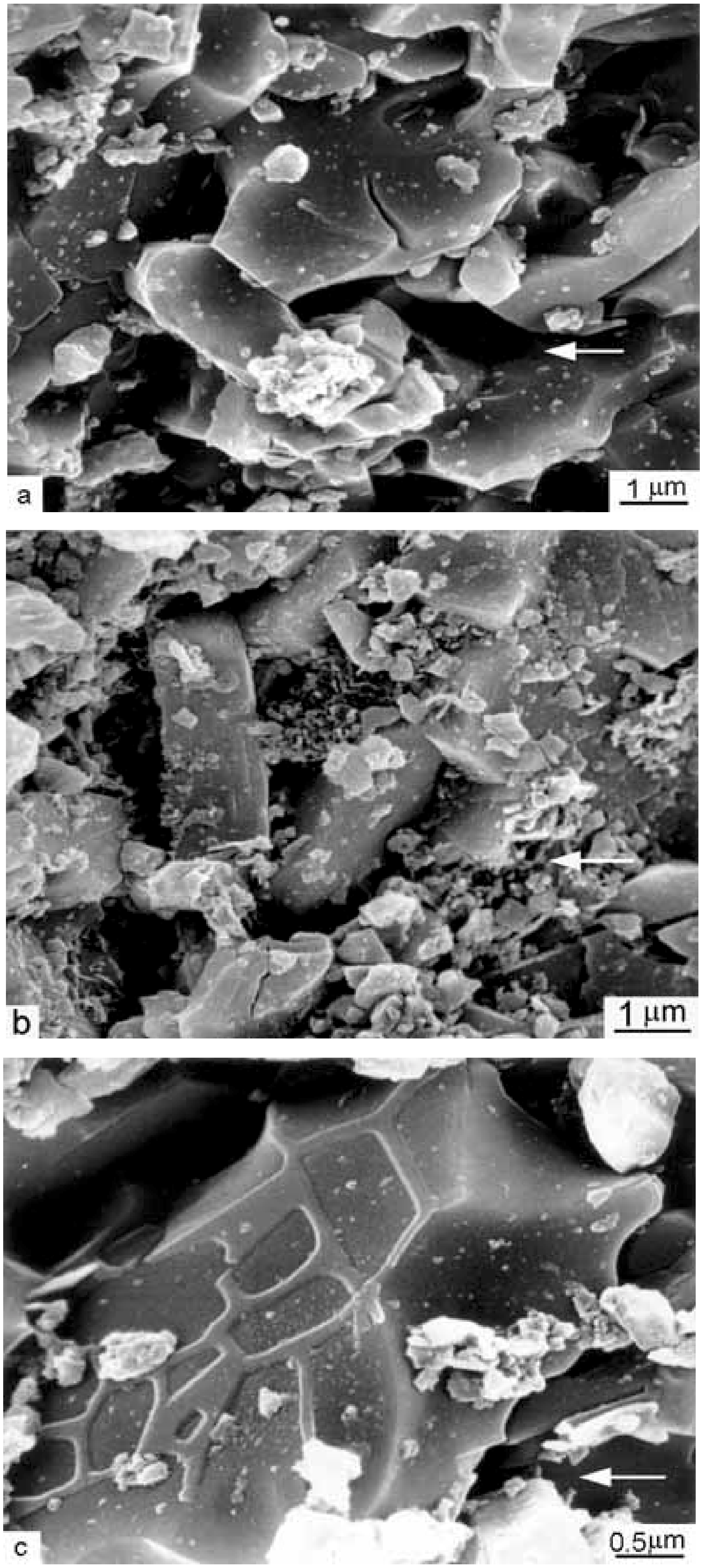

Fig. 9. Scanning electron micrographs fatigue fracture surfaces in ABC-SiC at 1300°C ($R$ = 0.1) for frequencies of (a) 25 Hz and (b) 3 Hz. Note the similarity to fatigue surfaces at 25°C (Fig. 8) with no evidence of glass phase formation on the crack surfaces. (c) Remains of the triple-junction grain-boundary phase can be seen in certain locations. Arrow indicates direction of crack growth.

largely unchanged between room temperature and 1300°C. Specifically, the grain-bridging mechanism seen at temperatures from ambient to as high as 1300°C occurs where the fracture is intergranular; the elastic and frictional tractions generated via the contact of opposing crack faces, during both initial debonding of the grain and subsequent frictional grain pullout, act to reduce the near-tip crack-driving force and hence retard subsequent crack extension. The basis for the cyclic component to fatigue-crack growth in these instances is the cycle-dependent, progressive suppression of such crack-tip shielding in the crack wake. The minimal effect of temperature and absence of any dependence of frequency on growth rates confirms the lack of a viscous component to such bridging in ABC–SiC.

### 4.2. *Role of microstructure*

Such behavior can be related to the nature of the grain-boundary amorphous phase and the transformations within this phase during prolonged exposure at elevated temperatures. At ambient temperatures, the grain boundaries in ABC–SiC

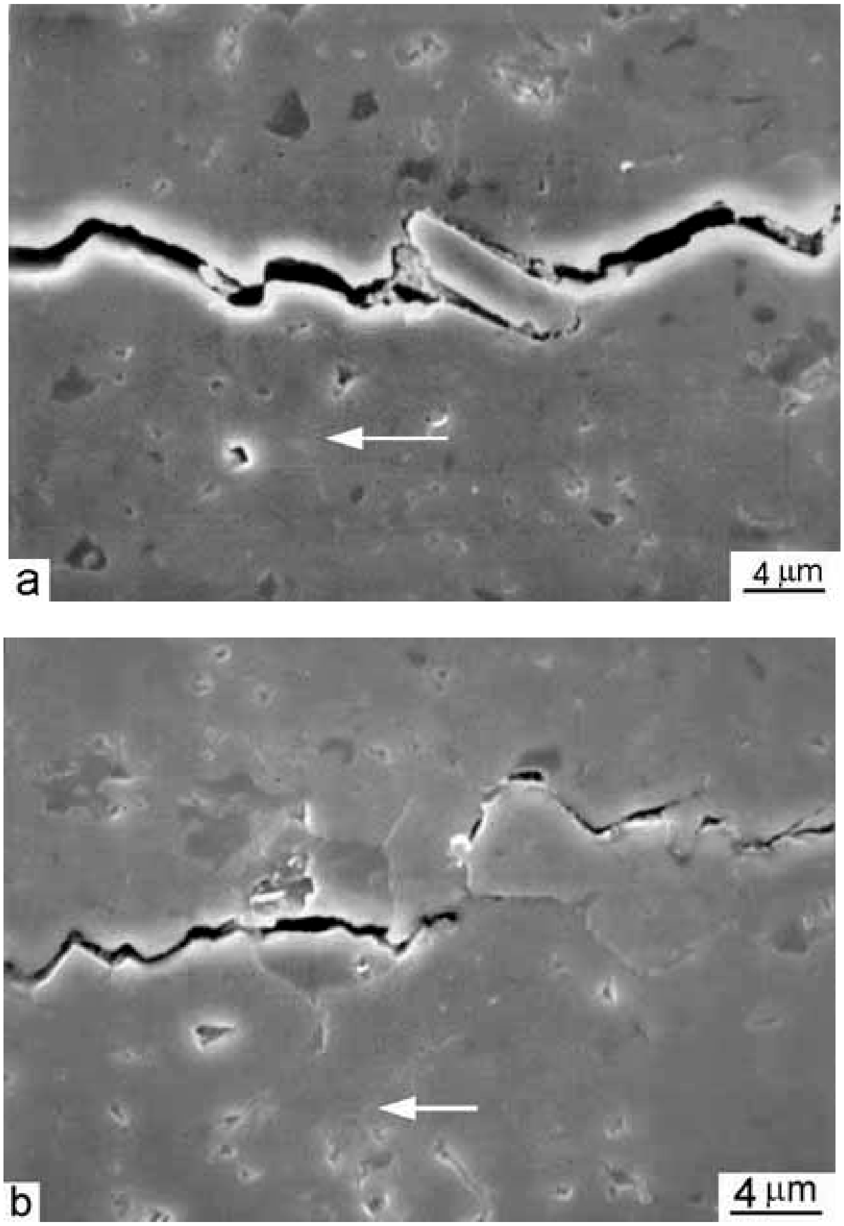

Fig. 10. Scanning electron micrographs of the profiles of fatigue cracks propagating at room temperature ($R = 0.1$) at (a) 25 Hz and (b) 1000 Hz. Note the intergranular crack path and bridging grains in the crack wake, with evidence of debris products resulting from frictional wear of such bridges during cyclic loading. Arrow indicates direction of crack growth.

after processing contain a ~1-nm thick Al- and O-rich amorphous film, with crystalline pockets at triple points. The existence of this phase promotes intergranular cracking, thereby enhancing grain bridging and the low-temperature fracture toughness. However, it is seldom easy to develop high temperature strength in a ceramic while maintaining such low-temperature toughness as the intergranular phase often becomes highly viscous at elevated temperatures; the resulting softening and cavitation at higher stresses and temperatures can lead to severe creep damage.

Clearly such phenomena are not occurring in ABC–SiC as the grain-boundary films are not becoming viscous at elevated temperatures such that the ambient-temperature mechanisms remain active up to 1300°C. High-resolution transmission electron microscopy studies in this work revealed that the thickness of the glassy film is significantly reduced due to crystallization following prolonged thermal exposure during the fatigue tests. Parallel studies on the creep properties of ABC–SiC at temperatures between 1100 and 1400°C have also indicated that substantial crystallization of amorphous

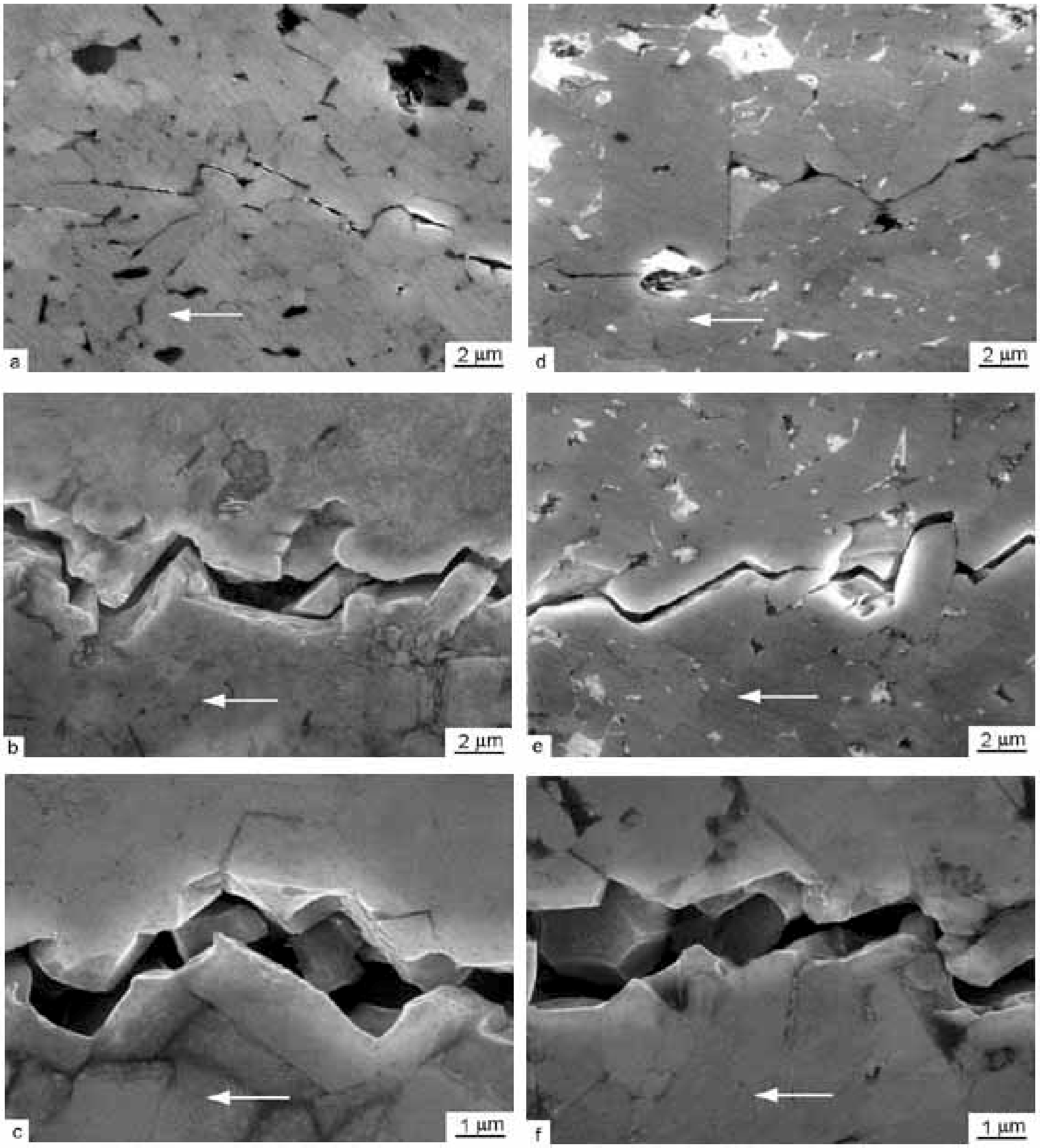

Fig. 11. Scanning electron micrographs of the profiles of fatigue cracks propagating at 1300°C ($R$ = 0.1) at (a–c) 3 Hz and (d–f) 25 Hz. Shown are (a,d) the crack-tip region, (b,e) ~150–200 μm behind the crack tip, and (c,f) ~1 mm behind the crack tip. Note the similarity to fatigue crack paths at room temperature. Arrows indicate direction of crack propagation.

phase occur [50]. Indeed, the grain-boundary phase appears to be fully crystalline, as shown in Fig. 13. The kinetics of this transformation are currently unknown, but it is clear that during the initial stages of elevated temperature testing, this microstructural evolution is highly beneficial to the crack-growth resistance of the material.

The consequences of this are that the mechanical properties change with initial exposure to temperatures above ~1100°C, due to the crystallization of glassy phase. This is clearly demonstrated for ABC–SiC, based on creep strength, fracture toughness and fatigue testing.

*4.2.1. Creep strength*. Following an initial primary creep stage with primary strain $\varepsilon_p \approx 0.001$, steady-state creep rates, $\dot{\varepsilon}$, in ABC-SiC are relatively low [50], i.e. $\dot{\varepsilon} < 2 \times 10^{-10}$ /s at 1200°C and $\dot{\varepsilon} = 6 \times 10^{-10}$ /s at 1300°C under the load of $\sigma = 100$ MPa. In comparison, the commercial ceramic SiC-Hexoloy exhibits far higher creep rates, i.e. $\varepsilon_p \approx 0.018$ and $\dot{\varepsilon} \approx 8.8 \times 10^{-9}$ /s at 1200°C ($\sigma = 139$ MPa). Similarly, in $Si_3N_4$-GN-10, creep rates are an order of magnitude faster, i.e. $\varepsilon_p \approx 0.009$, $\dot{\varepsilon} = 1.78 \times 10^{-9}$ /s at 1300°C ($\sigma = 100$ MPa) [51]. Moreover, the four-point bending strength at 1400°C was found to be increased from an initial strength of 100 MPa to 200 and 235 MPa following exposure at 1500°C for 24 and 48 h, respectively, prior to testing [50].

*4.2.2. Fracture toughness*. Fracture toughness values were also enhanced by prior high-temperature exposure. For as-processed ABC-SiC, $K_c$ toughness values measured on pre-cracked DC(T) specimens were 6.2 MPa√m at 25°C and 4.4 MPa√m at 1300°C. However, following 85 h of pre-exposure at 1300°C, these toughnesses were increased by ~16–20% to 7.2 MPa√m at 25°C and 5.2 MPa√m at 1300°C.

*4.2.3. Fatigue properties.* Likewise, pre-exposure at 1300°C for 85 hr had a marked effect on the fatigue-crack propagation properties at ambient temperatures. Compared to the as-processed condition, pre-exposure resulted in a shift of the

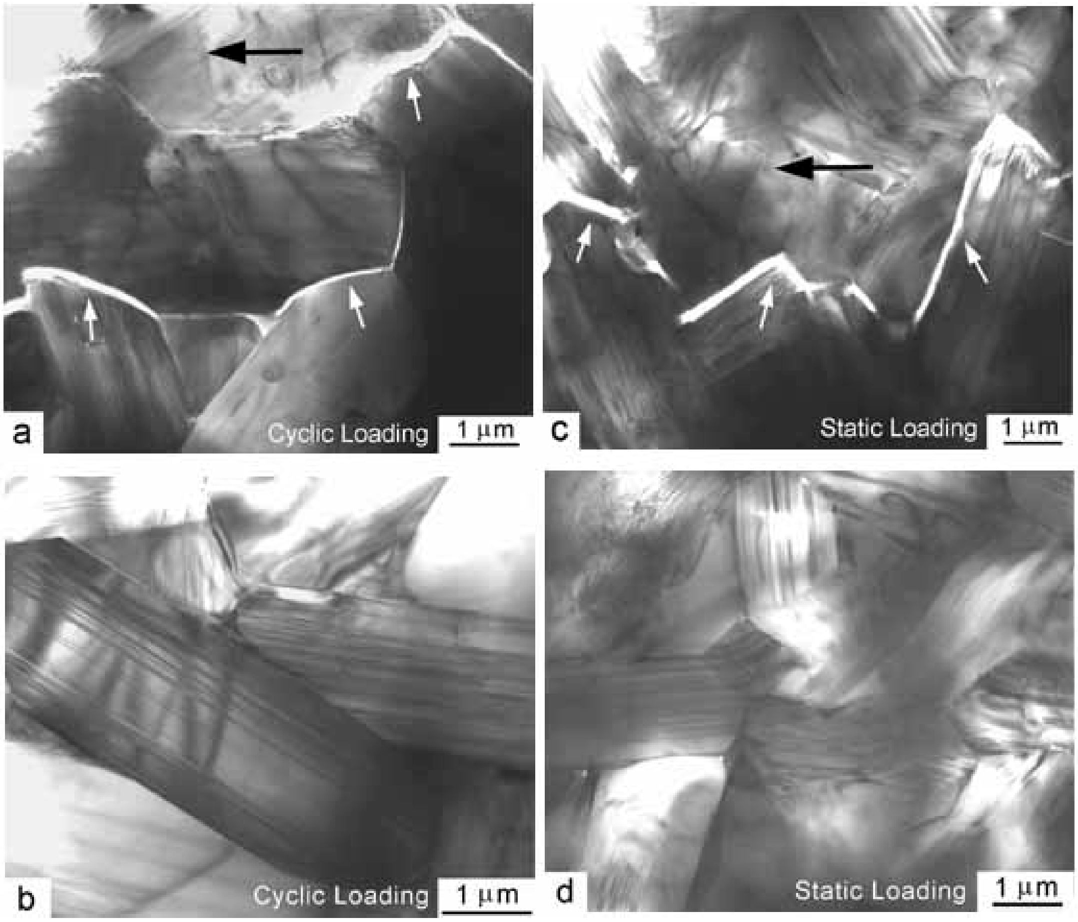

Fig. 12. Transmission electron micrographs of (a,c) the crack profiles and (b,d) microstructures near the crack tip in ABC–SiC at 1300°C under (a,b) cyclic loading ($R = 0.1$, $\nu = 25$ Hz, $K_{max} = 4.1$ MPa√m) and (c,d) sustained loading ($K_I = 4.1$ MPa√m). Large arrows indicate the general direction of crack propagation, and small arrows point to the primary cracks near the crack tip.

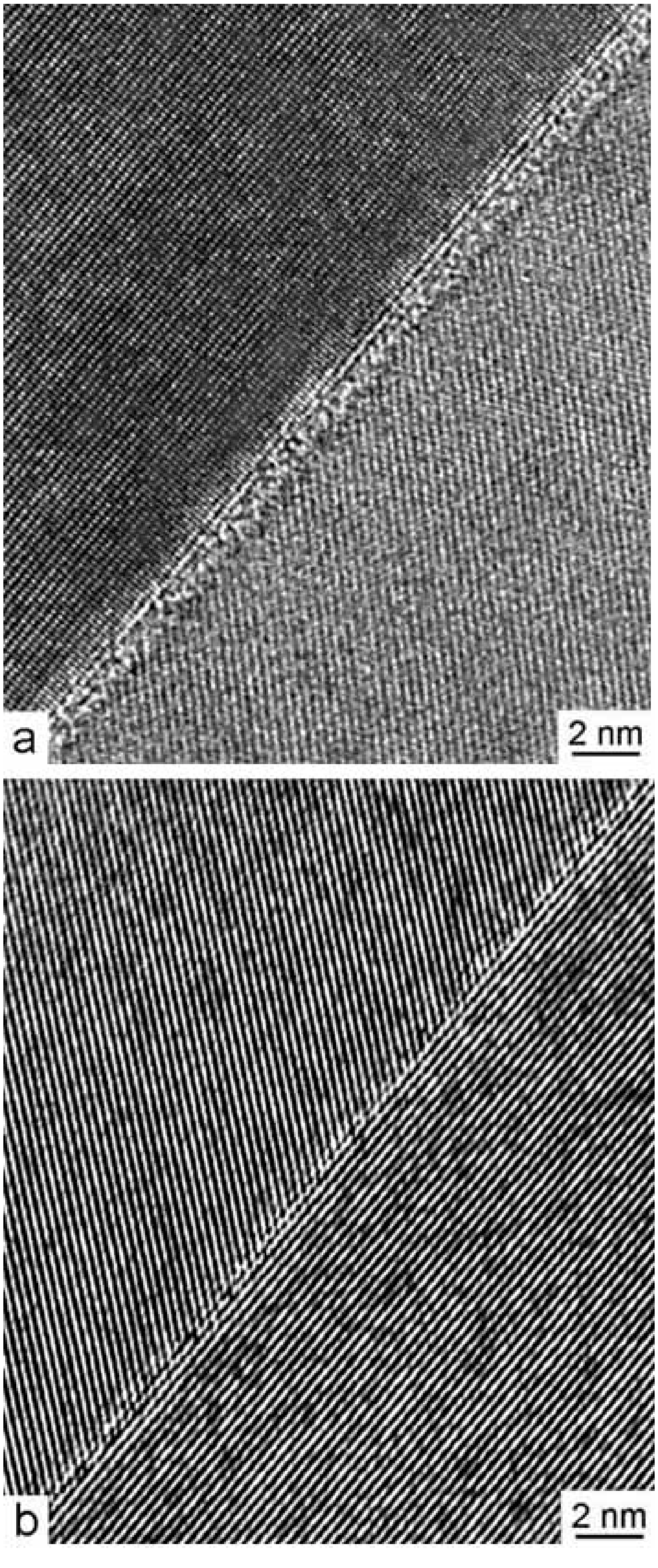

Fig. 13. High-resolution transmission electron micrographs of the grain boundaries in ABC–SiC in the (a) as-processed, and (b) thermally exposed (1300°C for ~72 h) conditions. Note the complete crystallization of the amorphous phase after exposure compared to the glass film of ~1 nm under as-processed condition.

entire growth-rate curve to a higher applied threshold stress-intensity range, $\Delta K_{th}$, from ~5.1 to 5.8 MPa√m ($R$ = 0.1, ν = 25 Hz), with no visible change in slope.

Such results are consistent with a recent study [52] on a SiC-reinforced silicon nitride composite at 1200°C, where crystallization of the grain-boundary glass phase produced a marked improvement in both cyclic and static crack-growth resistance at high temperatures, through reduced glass flow and crack-tip cavitation. Moreover, after such crystallization, fatigue-crack growth rates were independent on frequency between 2 and 20 Hz. Similarly, the literature is rich with examples where the crystallization of the grain-boundary phase leads to improved elevated temperature properties [53–56].

In the present study, even though the primary mechanisms of damage (intergranular cracking) and shielding (frictional wear of the grain-bridging zone) are apparently unchanged between 25 and 1300°C, fatigue-crack growth rates are increased and $\Delta K_{th}$ thresholds are some 30% lower at the higher temperature. This may be rationalized by considering models for grain bridging [57, 58] and the degradation of such bridging under cyclic loading due to frictional wear [14, 30]. The frictional pullout resistance from sliding along grain boundaries at the bridge-matrix interface can be represented by the relationship between the bridging stress, $p(u)$, and the crack-opening displacement, $2u$ [58]:

$$p(u) = \mu \cdot \sigma_N \, (1 - u/u_f)^n \tag{4}$$

where $\mu$ is the frictional coefficient between sliding grain faces, $\sigma_N$ is the normal stress acting on the interface, which can be equated to the residual stress resulting from thermal expansion anisotropy during cooling from the processing temperature, $2u_f$ is the critical crack opening for bridge rupture (typically equal to the grain height), and $n$ is an exponent governing the decrease in frictional stress with increase in $u$. Above ~800°C, the residual stresses will "anneal out" such that $\sigma_N$ will decrease with increasing temperature. Without structural or chemical changes in the grain-boundary phase such that the frictional coefficient remains roughly constant, the bridging stress will decrease with temperature, leading to a reduced crack-growth resistance. However, at temperatures above 1100–1200°C where crystallization can occur, the frictional coefficient may be expected to be increased, provided any remnant glassy phase does not become viscous. It is feasible that in this regime the decrease in $\sigma_N$ is compensated by the increase in $\mu$, consistent with the fact that the crack-growth resistance at 1300°C is marginally superior to that at 1200°C.

### 4.3. *Closing comments*

In many ceramics, microstructural development involves a compromise between low temperature toughness, which is promoted by the presence of the amorphous grain-boundary film, and high-temperature creep strength, where the amorphous phase can soften and become a preferred site for creep damage by cavitation. The present material appears to combine the "best of both worlds", where the intergranular amorphous phase, which gives rise to reasonable low temperature toughness, transforms by crystallization to a much more stable phase at elevated temperatures. Although this would occur *in situ* during high temperature service, akin to metals, this does suggest that the overall properties of many ceramics could be significantly improved by prior heat treatment.

## 5. CONCLUSIONS

Based on a study of elevated-temperature cyclic fatigue-crack propagation behavior in an *in situ* toughened monolithic silicon carbide with Al, B and C additions (ABC–SiC), involving the use of electrical-potential methods to continuously monitor crack growth *in situ* at temperatures between 25-1300°C, the following conclusions can be drawn:

1. With increasing temperature from 25 to 1200°C, fatigue-crack growth rates were increased and the $\Delta K_{th}$ threshold decreased by ~35% from 5.1 MPa√m at 25°C to 3.4 MPa√m at 1200°C ($R$ = 0.1, ν = 3–25 Hz). However, there was no further degradation in crack-growth resistance at 1300°C; growth rates and threshold values were essentially identical to those measured at 1200°C.
2. At all temperatures, growth rates showed a marked power-law dependence on the applied stress-intensity level; in terms of a simple Paris law representation, $da/dN \propto \Delta K^m$, the exponent $m$ varied at $R$ = 0.1 from 35 to 68, depending on the temperature and loading frequency.
3. Cyclic crack growth rates were found to be essentially independent of loading frequency, both at room temperature (25–1000 Hz) and surprisingly at elevated temperatures (3–25 Hz). Threshold $\Delta K_{th}$ values showed only a minimal 3–6% change, indicting that crack growth between 25 and 1300°C in this ceramic is predominantly cyclic- rather than time-dependent.
4. At fixed $\Delta K$ levels, growth rates are accelerated and thresholds $\Delta K_{th}$ reduced with increasing load ratio ($R$ = 0.1–0.5) at both 25 and 1300°C. This results from a predominant dependence of growth rates on $K_{max}$ rather than $\Delta K$ (i.e. $da/dN \propto K_{max}^{74}$) at both low and high temperatures. Consistent with this marked $K_{max}$-dependency, at the same $K_{max}$ level, crack velocities under cyclic loads were significantly faster than those under static loads at both 25 and 1300°C.
5. Mechanistically, crack-path profiles, fracture surface morphologies and TEM imaging of the

region directly ahead of the crack tip show a predominantly intergranular mechanism of crack advance at both low and high temperatures with crack-tip shielding by grain bridging in the crack wake; the existence of extensive wear debris on fatigue fracture surfaces furthermore suggests that such bridging is degraded under cyclic loading. No evidence of microcracking zones, creep cavitation nor any form of viscous-ligament bridging by the grain-boundary glassy phase was seen at any temperature studied up to 1300°C.

6. Such observed behavior strongly suggests that the damage and shielding mechanisms governing high-temperature fatigue-crack growth behavior in ABC–SiC up to ~1300°C are essentially unchanged from those at ambient temperatures. The absence of creep-induced softening and cavitation in the grain-boundary glassy layer, together with the occurrence of viscous-ligament bridging, is attributed to the microstructural evolution that occurs in ABC–SiC during the initial stages of high-temperature ( > 1100°C) exposure in the form of the crystallization of the grain-boundary glassy phase.

*Acknowledgements* — This work was supported by the Director, Office of Science, Office of Basic Energy Sciences, Materials Sciences Division of the U.S. Department of Energy under Contract No. DE-AC03-76SF00098. DC would additionally like to acknowledge the support of Berkeley Scholars Program in the form of a Tang Fellowship. Particular thanks are due to Mark Sixta and L. C. DeJonghe (who developed ABC-SiC) for help with the processing and for discussions on their parallel studies on creep in ABC–SiC, and to J. M. McNaney for his help with experimentation.

## REFERENCES

1. Becher, P. F., *J. Am. Ceram. Soc.*, 1991, **74**, 255.
2. Ritchie, R. O. and Dauskardt, R. H., *J. Ceram. Soc. Jpn.*, 1991, **99**, 1047.
3. Guiu, F., Reece, M. J. and Vaughan, D. A. J., *J. Mater. Sci.*, 1991, **26**, 3275.
4. Kishimoto, H., *JSME Int. J.*, 1991, **34**, 393.
5. Suresh, S., *J. Hard Mater.*, 1991, **2**, 29.
6. Dauskardt, R. H. and Ritchie, R. O., *Closed Loop*, 1989, **17**, 7.
7. Evans, A. G., *J. Am. Ceram. Soc.*, 1990, **73**, 187.
8. Cao, J. J., MoberlyChan, W. J., De Jonghe, L. C., Gilbert, C. J. and Ritchie, R. O., *J. Am. Ceram. Soc.*, 1996, **79**, 461.
9. Lee, S. K. and Kim, C. H., *J. Am. Ceram. Soc.*, 1994, **77**, 1655.
10. Padture, N. P., *J. Am. Ceram. Soc.*, 1994, **77**, 519.
11. Padture, N. P. and Lawn, B. R., *J. Am. Ceram. Soc.*, 1994, **77**, 2518.
12. Dauskardt, R. H., Yu, W. and Ritchie, R. O., *J. Am. Ceram. Soc.*, 1987, **70**, C248.
13. Dauskardt, R. H., Marshall, D. B. and Ritchie, R. O., *J. Am. Ceram. Soc.*, 1990, **73**, 893.
14. Lathabai, S., Rödel, J. and Lawn, B., *J. Am. Ceram. Soc.*, 1991, **74**, 1340.
15. Guiu, F., Li, M. and Reece, M., *J. Am. Ceram. Soc.*, 1992, **75**, 2976.
16. Hay, J. C. and White, K. W., *J. Am. Ceram. Soc.*, 1993, **76**, 1849.
17. Kishimoto, H., Ueno, A. and Okawara, S., *J. Am. Ceram. Soc.*, 1994, **77**, 1324.
18. Li, M. and Guiu, F., *Acta metall. mater.*, 1995, **43**, 1871.
19. Gilbert, C. J., Dauskardt, D. R., Steinbrech, R. W., Petrany, R. N. and Ritchie, R. O., *J. Mater. Sci.*, 1995, **30**, 643.
20. Gilbert, C. J., Dauskardt, R. H. and Ritchie, R. O., *J. Am. Ceram. Soc.*, 1995, **78**, 2291.
21. Corneliessen, B. E., Dauskardt, R. H., Ritchie, R. O. and Thomas, G., *Acta metall. mater.*, 1994, **42**, 3055.
22. Choi, G., Horibe, S. and Kawabe, Y., *Acta metall. mater.*, 1994, **42**, 1047.
23. Jacobs, D. S. and Chen, I. -W., *J. Am. Ceram. Soc.*, 1994, **77**, 1153.
24. Pezzotti, G., Okamoto, Y., Nishida, T. and Sakai, M., *Acta metall. mater.*, 1995, **43**, 1323.
25. Gilbert, C. J., Cao, J. J., MoberlyChan, W. J., De Jonghe, L. C. and Ritchie, R. O., *Acta metall. mater.*, 1996, **44**, 3199.
26. Gilbert, C. J. and Ritchie, R. O., *Acta. mater.*, 1998, **46**, 609.
27. Vekinis, G., Ashby, M. F. and Beaumont, P. W. R., *Acta metall. mater.*, 1990, **38**, 1151.
28. Steinbrech, R. W., Reichl, A. and Schaarwächter, W., *J. Am. Ceram. Soc.*, 1990, **73**, 2009.
29. Cai, H., Faber, K. T. and Fuller. Jr, E. R., *J. Am. Ceram. Soc.*, 1992, **75**, 3111.
30. Dauskardt, R. H., *Acta metall. mater.*, 1993, **41**, 2765.
31. Hu, X. Z., Lutz, E. H. and Swain, M. V., *J. Am. Ceram. Soc.*, 1991, **74**, 1828.
32. Jacobs, D. S. and Chen, I. -W., *J. Am. Ceram. Soc.*, 1995, **78**, 513.
33. Ewart, L. and Suresh, S., *J. Mater. Sci.*, 1992, **27**, 5181.
34. Liu, S. -Y., Chen, I-W. and Tien, T. -Y., *J. Am. Ceram. Soc.*, 1994, **77**, 137.
35. Hansson, T., Miyashita, Y. and Mutoh, Y., 1996, *Fracture Mechanics of Ceramics*, Vol. 12, *Fatigue, Composites and High Temperature Behavior* ed. Bradt, R. C. *et al.*, Plenum Press, New York, 187.
36. Lin, C. -K. J., Jenkins, M. G. and Ferber, M. K., *J. Mater. Sci.*, 1994, **29**, 3517.
37. Ramamurty, U., Hansson, T. and Suresh, S., *J. Am. Ceram. Soc.*, 1994, **77**, 2985.
38. Jenkins, M. G., Ferber, M. K. and Lin, C. K. J., *J. Am. Ceram. Soc.*, 1993, **76**, 788.
39. Zhang, Y. H. and Edwards, L., *Mater. Sci. Engng.*, 1998, **256A**, 144.
40. Lin, C. -K. J. and Socie, D. F., *J. Am. Ceram. Soc.*, 1991, **74**, 1511.
41. Liu, S. -Y. and Chen, I. -W, *Acta mater.*, 1996, **44**, 2079.
42. Evans, A. G., Russel, L. R. and Richerson, D. W., *Metall. Trans.*, 1975, **6A**, 707.
43. Blumenthal, W. and Evans, A. G., *J. Am. Ceram. Soc.*, 1984, **67**, 751.
44. Ramamurty, U., Kim, A. S. and Suresh, S., *J. Am. Ceram. Soc.*, 1993, **76**, 1953.
45. Ramamurty, U., *J. Am. Ceram. Soc.*, 1996, **79**, 945.
46. McNaney, J. M., Gilbert, C. J. and Ritchie, R. O., *Acta mater.*, 1999, **47**, 2809.
47. Morgan, J. M. and Milligan, W. W., In *Proceeding of the conference High Cyclic Fatigue of Structural Materials*, ed. Soboyeji, W. O. and Srivatsan, T. S. TMS, Warrendale, PA, 1997, p. 305.
48. Gilbert, C. J., McNaney, J. M., Dauskardt, R. H. and Ritchie, R. O., *ASTM J. Test. Eval.*, 1994, **22**, 117.
49. Dauskardt, R. H., James, M. R., Porter, J. R. and Ritchie, R.O., *J. Am. Ceram. Soc.*, 1992, **75**, 759.
50. Zhang, X. F., Sixta, M. and De Jonghe, L. C., private

communication, Lawrence Berkeley National Laboratory, 1999.

51. Ding, J. L., Liu, K. C., More, K. L. and Brinkman, C. R., *J. Am. Ceram. Soc.*, 1994, **77**, 867.
52. Zhang, Y. H., Edwards, L. and Plumbridge, W. J., *Acta mater.*, 1998, **46**, 1327.
53. Lange, F. F., Davis, B. I., and Metcalf, M. G., *J. Mater. Sci.*, 1983, **18**, 1497.
54. Cinibulk, M. K., Thomas, G., and Johnson, S. M., *J. Am. Ceram. Soc.*, 1992, **75**, 2037.
55. Cinibulk, M. K., Thomas, G., and Johnson, S. M., *J. Am. Ceram. Soc.*, 1992, **75**, 2044.
56. Becker, P. F., Hwang, S. L., and Hsueh, C. H., *MRS Bulletin*, 1995, **20**, 23.
57. Lawn, B. R., *Fracture of Brittle Solids*, 2nd ed., Cambridge University Press, New York, 1993.
58. Foote, R. M. L., Mai, Y.-W. and Cotterell, B., *J. Mech. Phys. Solids*, 1986, **34**, 593.
59. Riedel, H. and Rice, J. R., in *Fracture Mechanics: Twelfth Conference, ASTM Special Technical Publication 700*, ed. P. C. Paris. American Society for Testing and Materials, Philadelphia, PA, 1980, p. 112.
60. Kumar, V., German, M. D. and Shih, C. F., *An Engineering Approach for Elastic-Plastic Fracture Analysis*, EPRI Topical Report No. NP-1931, Electric Power Research Institute, Palo Alto, CA, 1981.

## APPENDIX A

### *A1. Justification for the use of the stress intensity K at elevated temperatures*

To justify the use of the linear-elastic stress intensity $K$ to characterize crack growth at elevated temperatures, the relative magnitudes of the fatigue cycle time, $t_c$, i.e. the duration of the fatigue cycle, $t_c = 1/\nu$, where $\nu$ is the frequency, and the transition time, $t_T$, which governs the transition from small-scale creep to extensive creep at the crack tip, were compared. Small-scale creep conditions exist when $t_c \ll t_T$; under these conditions, fatigue-crack growth is essentially controlled by the mechanical loads, i.e. the stress intensity factor $K$ (for static fracture) or its range $\Delta K$ (for cyclic loading conditions). The transition time is expressed in terms of $K_{\max}$ the maximum stress intensity in the cycle [59]:

$$t_T = \frac{(1-\upsilon^2)K_{\max}{}^2}{(q+1)EC*} \tag{A1}$$

where $\upsilon$ is Poisson's ratio, $q$ is the power-law creep exponent, $E$ is Young's modulus, and $C*$ is the steady-state creep parameter (a rate-dependent analog of $J$), which is given by [60]:

$$C* = \dot{\varepsilon}_0 \sigma_0 (W-a)(P/P_0)^{n+1} h(q, \text{geometry}) \tag{A2}$$

where $\dot{\varepsilon}_0$ is the reference creep strain rate, $\sigma_o$ is the reference strength, $W$ is the width of specimen, $a$ is the crack length, $P$ is the applied load, $P_o$ is the reference load, and $h$ is a dimensionless function dependent on $q$ and specimen geometry.

For the ABC–SiC ceramic, the values of the power-law creep exponent $q$ and constant $A$ are 0.77 and $1.76\times10^{-11}$ MPa$^{-n}$ s$^{-1}$, respectively [50]. Using equations (2) and (3) with $\upsilon = 0.2$, $E$ = 400 GPa, $K_{\max}$ = 4.5 MPa√m, $\sigma_o$ = 620 MPa, $W$ = 28 mm and $a$ = 14 mm, a conservative estimate of the transition time $t_T$ is ~2500 s. Since at the lowest frequency used of 3 Hz the fatigue cycle time $t_c$ is 0.33 s, we conclude that since $t_c \ll t_T$ for all tests, the stress intensity $K$ is an appropriate parameter to characterize crack growth in the present work.

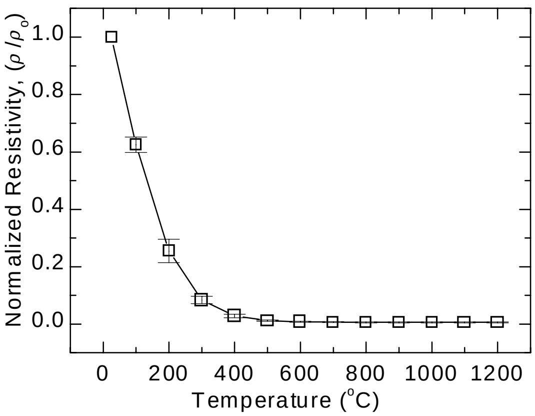

Fig. A1. Relationship between electrical resistivity and temperature in ABC–SiC, where $\rho_o$ is the resistivity at room temperature.

## APPENDIX B

### *B1. Electrical potential-drop crack length monitoring in ceramics*

The electrical potential-drop technique operates on the concept that if a constant current is passed through a test specimen containing a crack, its electrical resistance (and hence the voltage measured across the crack) will increase with increase in crack length. Since the basic requirement is that the test material must be conductive, this rules out most structural ceramics. Thin metallic films can be affixed to the surface of non-conducting specimens and, although this works well at ambient temperatures [6, 12], it is generally unsuitable for operation above ~900°C. Silicon carbide, however, does display some degree of electrical conductivity. At room temperature, its electrical resistivity ($\rho$ = ~ $10^4$ Ω cm) is too high to use the technique effectively. At elevated temperatures, on the other hand, there is roughly three orders magnitude decrease in the resistivity ($\rho$ = ~ $10^1$ Ω cm above 600°C), as shown in Fig. A1. Since the electrical resistance between two potential measurement leads located ~1 mm above and below the notch in, say, a compact-tension specimen is now 20–50 Ω, the electrical-potential crack monitoring technique can be readily employed using standard calibrations [48].